Journal of Applied Electrochemistry **30**: 1321–1333, 2000.

Impact of chlorine and acidification in the electrochemical treatment of tumours†

E. NILSSON[1]*, J. BERENDSON[1] and E. FONTES[2]
[1]*Catella Generics AB Veddestavägen 7, SE-17562 Järfälla, Sweden*
[2]*Comsol AB, Tegnérgatan 23, SE-11140 Stockholm, Sweden*
*(*author for correspondence, phone: +46 8445 7975, fax: +46 8445 7999, e-mail: eva.n@cgr.se)*

Received 26 July 1999; accepted in revised form 23 November 1999

Key words: chlorine, direct current, electrochemical treatment (EChT), mathematical modelling, tumour

Abstract

Electrochemical treatment (EChT) of tumours offers considerable promise as a safe, simple and relatively noninvasive antitumour therapy. When platinum is used as electrode material, the major electrochemical reactions at the anode are chlorine and oxygen evolution. Conflicting opinions can be found in the literature over the role of chlorine in the underlying destruction mechanism behind EChT. In this present study, the impact of chlorine in EChT treatments is investigated by means of mathematical modelling. The analysis focuses on the tissue surrounding a spherical platinum anode when applying a constant current density. Tissue is modelled as an aqueous solution of sodium chloride containing a bicarbonate buffer system and organic constituents susceptible to reactions with chlorine. Except for the case of very low anode current densities, the simulations clearly show that it is the spreading of hydrogen ions – and not chlorine molecules – that determines the extent of tissue destruction around the anode. Moreover, it is found that the reactions of chlorine with tissue play important roles as generators of hydrogen ions. The contribution of these reactions to the acidification of tissue, surrounding the anode, is strongly dependent on the applied current density and increases with decreasing current density.

1. Introduction

Electrochemical treatment (EChT) has shown promise as a safe, simple and relatively noninvasive antitumour therapy for treatment of localized malignant as well as benign tumours. Direct current is passed through two or more electrodes placed inside the tumour, or close to its vicinity, and lesions are produced in distinct regions centred on each of the electrodes. Several contributory factors are involved in the tissue destruction, although their respective roles in producing the antitumour effect are not yet fully understood [1–5]. However, the primary destruction of the tissue surrounding the electrodes is most probably caused by toxic species produced in the electrochemical reactions [1, 3, 6].

Platinum is the most widely used electrode material in EChT treatments. When used is biological tissue, the main reactions at the anode are oxygen and chlorine evolution:

$$2\,H_2O \rightleftharpoons O_2 + 4\,H^+ + 4\,e^- \quad (1)$$

$$2\,Cl^- \rightleftharpoons Cl_2 + 2\,e^- \quad (2)$$

The major electrochemical reaction at the cathode is hydrogen evolution:

$$2\,H_2O + 2\,e^- \rightleftharpoons H_2 + 2\,OH^- \quad (3)$$

Consequently, the dominating reaction products, which are locally destructive at the anode, are hydrogen ions and various species containing oxygen and chlorine. Hydroxyl ions and molecular hydrogen are the destructive reaction products at the cathode.

EChT has not yet been universally accepted despite the fact that more than ten thousand tumour patients have been treated in China during the past ten years [7–9]. The reason for this is the lack of basic preclinical studies and reliable clinical trials. Uncertainties regarding the destruction mechanism of EChT also hinder the development of an optimized dose planning methodology. Therefore, a useful tool in investigating the underlying destruction mechanisms behind EChT, as well as in developing a dose planning strategy, is mathematical modelling. A mathematical model of the electrolysis process can be used to simulate concentration profiles, of substances dissolved in tissue, and the potential profile within the tissue, both as a function of time. Moreover, if a correlation between the simulated profiles and destructive effect, obtained in experiments,

† Dedicated to the memory of Daniel Simonsson

can be found the model can be used to predict the size of lesions produced through EChT.

Two simplified mathematical models of the electrochemical processes, occurring during EChT, have been formulated and visualized [10, 11]. The models focused on the tissue surrounding a spherical platinum anode when applying a constant direct current. The models were based on transport equations of ionic species in dilute solutions. kinetic expressions for the electrochemical reactions were introduced at the anode surface. In the first model [11], tissue was treated as an aqueous solution of sodium chloride. The considered electrochemical reactions were the chlorine and oxygen evolution reactions while the considered homogeneous chemical reaction was the water protolysis reaction. In a second paper [10], the model was extended to take into account the limiting effect that the bicarbonate buffer system has on the spreading of hydrogen ions produced at the anode. The validity of the model was investigated by comparing simulated pH profiles with pH profiles reported from *in vivo* experiments [6]. The model was shown to give a very good qualitative and a fairly good quantitative description of the pH profile obtained in tissue surrounding the anode after EChT treatment. The discrepancy between simulations and experiments, in these earlier studies, could be attributed to other sources producing hydrogen ions, apart from the reaction of oxygen evolution. Such sources of hydrogen ions could originate from the reactions of chlorine with water and organic tissue constituents. Hence, a natural step in the refinement of the model is to implement to it the transport and reaction processes of chlorine.

Conflicting opinions can be found in the literature over the role of chlorine in the destruction of tissue around the anode. Samuelsson et al. stated that chlorine, through its oxidative properties, is the main agent responsible for the tissue destruction obtained in EChT treatments [4, 12]. Nordenström stressed that chlorine has no effect on the devitalisation of tissue surrounding the anode and instead, the spreading of hydrogen ions, stemming from the oxygen evolution reaction, is the primary destructive agent [1]. Li et al. suggested that the reaction of chlorine with water is the main source of hydrogen ions in tissue surrounding the anode [3]. Berendson et al. presented several primary estimations of the spreading of chlorine and hydrogen ions, in tissue surrounding a platinum electrode, during EChT [13, 14]. Their results are in line with Nordenström's opinion and indicate that the spreading of hydrogen ions, originating from the oxygen evolution reaction, determines the extent of the destruction zone around the anode.

The aim of this study is to elucidate the role of chlorine in the underlying destruction mechanisms behind EChT. This is done by further developing our mathematical model, presented in previous studies [10, 11], to also take into account the transport and reaction process of chlorine. The analysis focuses on the relative spreading of the chlorinated and acidic zones around the anode, as well as the role of chlorine as a source for production of hydrogen ions. To investigate the validity of the model, simulated pH and chlorine profiles are compared with pH profiles and lesion sizes reported from *in vivo* experiments [6].

2. Chlorine chemistry

Molecular chlorine, produced in the chlorine evolution reaction at the anode during EChT, reacts rapidly with water according to the following disproportionation reaction:

$$Cl_2(aq) + H_2O \rightleftharpoons HClO + H^+ + Cl^- \quad (4)$$

The equilibrium constant for this reaction is 6.3×10^{-4} M^2 at 37 °C [15]. Hypochlorous acid (HClO) is a weak acid that dissociates with a dissociation constant of 3.4×10^{-8} M at 37 °C [15]:

$$HClO \rightleftharpoons H^+ + OCl^- \quad (5)$$

Hence, at a chloride concentration of 0.13 M and pH < 2, Cl_2(aq) is the dominant species. HClO is the major species at $2 <$ pH < 7.2 and the hypochlorite ion (ClO^-) is dominant at pH > 7.2. In this study, the concentration of ClO^- in chlorinated tissue is considered to be negligible. This assumption is justified by the fact that pH is always <7.2 in tissues adjacent to the anode during EChT treatment.

Cl_2(aq) and HClO are highly reactive and are known to have strong toxic effects [16]. A schematic list of the principal chemical reactions of Cl_2(aq) and HClO, with organic constituents in aqueous solutions, is presented in Table 1. The reactions may be divided into three

Table 1. Principal reactions of Cl_2(aq) and HClO with organic compounds in aqueous solutions [16–20]

Type of reactions	Molecular chlorine	Hypochlorous acid
Addition	$RC = CR' + Cl_2(aq) + H_2O \rightarrow RC(Cl)C(OH)R' + H^+ + Cl^-$	$RC = CR' + HClO \rightarrow RC(Cl)C(OH)R'$
Substitution	$RH + Cl_2(aq) \rightarrow RCl + H^+ + Cl^-$	$RH + HClO \rightarrow RCl + H_2O$
Oxidation	$Cl_2(aq) + 2e^- \rightarrow 2Cl^-$ $R(red)\,(+H_2O)^* \rightarrow R(ox) + 2H^+ + 2e^-$	$H^+ + HClO + 2e^- \rightarrow H_2O + Cl^-$ $R(red)\,(+H_2O)^* \rightarrow R(ox) + 2H^+ + 2e^-$
	overall reaction: $Cl_2(aq) + R(red)\,(+H_2O)^* \rightarrow R(ox) + 2H^+ + 2Cl^-$	overall reaction: $HClO + R(red) \rightarrow R(ox) + H^+ + Cl^-\,(+H_2O)^*$

* Depending on its nature, the reaction may involve consumption or production of water

general groups; addition, substitution and oxidation. Addition reactions occur when Cl_2(aq) and HClO add across reactive organic double bonds. The major reaction products from aqueated chlorine addition reactions are chlorohydrin compounds [17, 18]. Substitution reactions involve the replacement of one atom or functional group with another. Cl_2(aq) and HClO react with aromatic and amino compounds to replace a hydrogen substituent and form C-chlorinated and N-chlorinated compounds [19]. In addition to acting as chlorinating agents, Cl_2(aq) and HClO also act as oxidising agents. Oxidation of an organic compound corresponds to increasing its oxygen content or to decreasing its hydrogen content. Oxidation of the organic compounds may take place with or without degradation of the compounds and both chlorinated and nonchlorinated compounds are subject to oxidation. Depending on the nature of the reaction, oxidation may involve either a consumption or production of water. Carbohydrates and carbohydrate-related compounds are examples of organics that are subject principally to oxidative reactions [20]. Cl_2(aq) and HClO may also oxidize inorganic constituents in tissue, such as iron and bicarbonate ions [15, 16]. However, these reactions are considered to be of negligible importance in comparison with the organic oxidation reactions.

The reactions of Cl_2(aq) and HClO with organic constituents in tissue are very complex. To account for the production of hydrogen and chloride ions from the reactions of Cl_2(aq) and HClO with organic matter, the following groups of reactions were treated in our model:

$$Cl_2(aq) + Org \rightarrow Org\text{—}Cl + Cl^- + H^+ \quad (6)$$

$$HClO + Org \rightarrow Org\text{—}Cl + H_2O \quad (7)$$

$$Cl_2(aq) + Org\text{–}red + H_2O \rightarrow Org\text{–}ox + 2\,Cl^- + 2\,H^+ \quad (8)$$

$$HClO + Org\text{–}red \rightarrow Org\text{–}ox + Cl^- + H^+ \quad (9)$$

In the above reactions, Org denotes an organic molecule susceptible to chlorination while Org–ox and Org–red denote an organic compound in its oxidised and reduced state, respectively. Reactions 6 and 7 represent all chlorinating reactions of Cl_2(aq) and HClO. No distinction is made between chlorination due to addition or substitution reactions. This simplification is justified by the fact that the addition and substitution processes of Cl_2(aq), both generate one chloride and hydrogen ion, while no ions are produced in the two processes involving HClO, see Table 1. Reactions 8 and 9 represent the oxidation reactions of Cl_2(aq) and HClO. It is assumed that all oxidation reactions involve an increase of the oxygen content of the organic compound and that only nonchlorinated organic compounds are subject to oxidation. Moreover, the oxidation reactions are assumed to proceed without degradation of the organic compound.

3. Problem definition and basic assumptions

The analysis is focused on the tissue around a spherical platinum anode when a direct current is applied. The spherical geometry of the model and the symbols used to denote its geometrical dimensions are illustrated in Figure 1. The electrolyte domain, Ω, is bounded by an inner and outer spherical surface. The inner boundary surface, $\partial\Omega_a$, represents the spherical anode with a radius r_a. The outer boundary, $\partial\Omega_r$, represents a spherical surface with a radius r_r, at a distance large enough from the anode to assure constant concentrations. The cathode is assumed to be placed at a distance far enough from the anode to ensure that the anodic and cathodic reaction zones do not interact.

Tissue is treated as a homogeneous aqueous solution of sodium chloride containing a bicarbonate buffer system. In addition it is considered to contain two types of organic constituents, Org and Org–red, which are susceptible to chlorination and oxidation, respectively.

It should be emphasized that real tissue is a heterogeneous medium containing a discontinuous cellular phase and a continuous extracellular phase. When current is applied to tissue, it is mainly transported through the channels of extracellular fluid. This is confirmed by the electroosmotic effects, which have shown to arise during EChT [1]. In this work, the transport of current is assumed to occur solely through the extracellular fluid. The cells serve as obstacles for the transport of species in the extracellular fluid and, in order to take into account the structure of tissue, effective mobilities, which include porosity and turtuosity as parameters, should be introduced. However, the effective transport properties in tissue are not known and it is out of the scope of this paper to determine these entities. The diffusion coefficients, of the involved species, have therefore been estimated to being those that occur in aqueous solutions.

There are a number of charged species present in low concentrations in extracellular fluids, that are not taken into account in the model (e.g., potassium). These

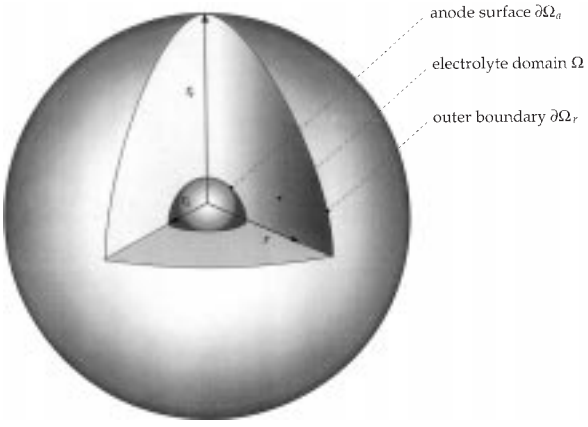

Fig. 1. Spherical geometry of the model and symbols used to denote its dimensions.

species, which in many cases have mobilities in the order of magnitude as sodium, should not have any larger influence on the simulation results. The buffer capacity of proteins is not considered in this work but will be introduced in a later study.

The model is based on the transport equations of ionic species, in dilute solutions, and the equations of electrode kinetics. A detailed derivation of the basic transport and electrode Kinetics equations is presented in an earlier article [11]. Inputs to the model are the current density, applied at the anode, and the sizes of the anode and electrolyte domain. Outputs from the model are concentration profiles of substances dissolved in tissue and the potential profile, as a function of time. In addition, current yields from the anode reactions are obtained from the model.

The considered electrochemical reactions are oxygen (1) and chlorine (2) evolution. In addition, eight homogenous chemical reactions are considered in the analysis. $Cl_2(aq)$, produced in the chlorine evolution reaction, hydrolyses according to Reaction 4. The substitution and addition reactions of $Cl_2(aq)$ and HClO, with organic constituents in tissue, are modelled using the simplified Reactions 6 and 7, while the oxidative reactions are modelled according to Reactions 8 and 9. Reactions 6, 7 and 9 are assumed to follow second-order rate laws, while Reaction 8 is assumed to be a pseudo-second order reaction. The four families of reactions of $Cl_2(aq)$ and HClO with organic species are assumed to be irreversible. Org and Org–red are immobile and both contain one reaction site each. The concentration of $Cl_2(aq)$ is limited by its saturation concentration at 1 atm. When the saturation concentration is exceeded, small chlorine bubbles, with an internal pressure of 1 atm, are assumed to be in equilibrium with $Cl_2(aq)$:

$$Cl_2(aq) \rightleftharpoons Cl_2(g) \tag{10}$$

Acidification of tissue surrounding the anode is counteracted by the bicarbonate buffer system in accordance to the following reaction:

$$H^+ + HCO_3^- \rightleftharpoons CO_2(aq) + H_2O \tag{11}$$

The concentration of $CO_2(aq)$ is assumed to be constant throughout the solution domain, and the validity of this assumption is discussed in [10]. Finally, hydrogen and hydroxyl ions react through the water protolysis reaction:

$$H^+ + OH^- \rightleftharpoons H_2O \tag{12}$$

A number of further assumptions, in addition to those mentioned above, are made in order to facilitate the problem's solution. These assumptions are:

(i) Two mechanisms, diffusion and migration, are assumed to contribute to the transport of the solute species in the tissue. The flux of species due to convection is neglected.
(ii) The solution near the electrode is assumed to be saturated with respect to oxygen. Small oxygen gas bubbles, with an internal pressure of 1 atm, are assumed to be in equilibrium with the platinum electrode surface.
(iii) The bubbles of chlorine and oxygen do not influence the conductivity of the electrolyte.
(iv) Drying effects caused by electroosmosis are neglected.

4. Model equations

The model includes ten unknowns; namely, nine concentrations (c_{Na^+}, c_{H^+}, c_{Cl^-}, c_{OH^-}, $c_{HCO_3^-}$, $c_{Cl_2(aq)}$, c_{HClO}, c_{Org}, $c_{Org-red}$) and the potential field ($\mathbf{\Phi}$). Consequently, ten model equations are, respectively, required in the electrolyte domain and each of the boundaries.

4.1. *Domain equations*

Differential material balances are formulated for all nine species in the electrolyte domain, Ω:

$$\frac{\partial c_i}{\partial t} = D_i \nabla^2 c_i + \frac{z_i}{|z_i|} u_i \nabla \cdot (c_i \nabla \mathbf{\Phi}) + R_i \tag{13}$$

where t denotes time, D_i the diffusion coefficient, u_i the ionic mobility and z_i the electrical charge of species i. R_i represents the production of a species through homogenous chemical reactions and is given by the following expressions.

$$R_{Na^+} = 0 \tag{14}$$

$$\begin{aligned} R_{H^+} = {} & k_{4,f} c_{Cl_2(aq)} - k_{4,b} c_{HClO} c_{H^+} c_{Cl^-} \\ & + k_{6,f} c_{Cl_2(aq)} c_{Org} + 2k_{8,f} c_{Cl_2(aq)} c_{Org-red} \\ & + k_{9,f} c_{HClO} c_{Org-red} - k_{11,f} c_{H^+} c_{HCO_3^-} \\ & + k_{11,b} c_{CO_2(aq)} c_{H_2O} - k_{12,f} c_{H^+} c_{OH^-} + k_{12,b} c_{H_2O} \end{aligned} \tag{15}$$

$$\begin{aligned} R_{Cl^-} = {} & k_{4,f} c_{Cl_2(aq)} - k_{4,b} c_{HClO} c_{H^+} c_{Cl^-} + k_{6,f} c_{Cl_2(aq)} c_{Org} \\ & + 2k_{8,f} c_{Cl_2(aq)} c_{Org-red} + k_{9,f} c_{HClO} c_{Org-red} \end{aligned} \tag{16}$$

$$R_{OH^-} = -k_{12,f} c_{H^+} c_{OH^-} + k_{12,b} c_{H_2O} \tag{17}$$

$$R_{HCO_3^-} = -k_{11,f} c_{H^+} c_{HCO_3^-} + k_{11,b} c_{CO_2(aq)} c_{H_2O} \tag{18}$$

$$\begin{aligned} R_{Cl_2(aq)} = {} & -k_{4,f} c_{Cl_2(aq)} + k_{4,b} c_{HClO} c_{H^+} c_{Cl^-} \\ & - k_{6,f} c_{Cl_2(aq)} c_{Org} - k_{8,f} c_{Cl_2(aq)} c_{Org-red} \\ & - k_{10,f} \left(c_{Cl_2(aq)} - c^s_{Cl_2(aq)} \right) \end{aligned} \tag{19}$$

$$\begin{aligned} R_{HClO} = {} & k_{4,f} c_{Cl_2(aq)} - k_{4,b} c_{HClO} c_{H^+} c_{Cl^-} \\ & - k_{7,f} c_{HClO} c_{Org} - k_{9,f} c_{HClO} c_{Org-red} \end{aligned} \tag{20}$$

$$R_{\mathrm{Org}} = -k_{6,\mathrm{f}} c_{\mathrm{Cl_2(aq)}} c_{\mathrm{Org}} - k_{7,\mathrm{f}} c_{\mathrm{HClO}} c_{\mathrm{Org}} \quad (21)$$

$$R_{\mathrm{Org-red}} = -k_{8,\mathrm{f}} c_{\mathrm{Cl_2(aq)}} c_{\mathrm{Org-red}} - k_{9,\mathrm{f}} c_{\mathrm{HClO}} c_{\mathrm{Org-red}} \quad (22)$$

Here, $k_{j,\mathrm{f}}$ and $k_{j,\mathrm{b}}$ denote the forward and backward rate constants of the homogeneous reaction j. The last term in Equation 19 represents the production of $Cl_2(g)$, which commences as soon as $c_{\mathrm{Cl_2(aq)}}$ exceeds its saturation concentration, $c^{\mathrm{S}}_{\mathrm{Cl_2(aq)}}$. Thus, $k_{10,\mathrm{f}}$ can be considered as a 'switching function' of $c_{\mathrm{Cl_2(aq)}}$:

$$k_{10,\mathrm{f}} = \exp\left\{\frac{c_{\mathrm{Cl_2(aq)}} - c^{\mathrm{S}}_{\mathrm{Cl_2(aq)}}}{a c^{\mathrm{S}}_{\mathrm{Cl_2(aq)}}}\right\} \quad (23)$$

The constant a is chosen so that $k_{10,\mathrm{f}} \to 0$ when $c_{\mathrm{Cl_2(aq)}} < c^{\mathrm{S}}_{\mathrm{Cl_2(aq)}}$ and $k_{10,\mathrm{f}} \to \infty$ when $c_{\mathrm{Cl_2(aq)}} > c^{\mathrm{S}}_{\mathrm{Cl_2(aq)}}$. The final equation within the domain is that of electroneutrality:

$$\sum_i z_i c_i = 0 \quad (24)$$

4.2. *Boundary and initial conditions*

Mass transport of species i across the anode surface, $\partial\Omega_{\mathrm{a}}$, is either nonexistent or equal to the charge transfer, present through virtue of the electrochemical reactions. Thus,

$$-D_i(\nabla c_i \cdot \mathbf{n}) - \frac{z_i}{|z_i|} u_i c_i (\nabla \boldsymbol{\Phi} \cdot \mathbf{n}) = \frac{v_{ij} i_j}{n_j F} \quad (25)$$

where $\mathbf{n}$ is the outward unit normal vector, n_j the number of electrons transferred in the electrochemical reaction j, v_{ij} the stoichiometric coefficient and F is the faradaic constant. i_j denotes the current density contributed by the electrochemical reaction j and are given by:

$$i_1 = i_{0,1}\left\{\exp\left[-\frac{F(\boldsymbol{\Phi} + E^{\mathrm{ref}}_{\mathrm{eq},1})}{2RT}\right] - (P_{\mathrm{O_2}})^{1/4} C_{\mathrm{H^+}} \exp\left[\frac{F(\boldsymbol{\Phi} + E^{\mathrm{ref}}_{\mathrm{eq},1})}{2RT}\right]\right\} \quad (26)$$

$$i_2 = i_{0,2}\left\{(C_{\mathrm{Cl^-}})\exp\left[-\frac{F(\boldsymbol{\Phi} + E^{\mathrm{ref}}_{\mathrm{eq},2})}{2RT}\right] - \left(C_{\mathrm{Cl_2(aq)}}\right)^{1/2} \exp\left[\frac{F(\boldsymbol{\Phi} + E^{\mathrm{ref}}_{\mathrm{eq},2})}{2RT}\right]\right\} \quad (27)$$

where $P_i = p_i/p^{\mathrm{ref}}_i$ and $C_i = c_i/c^{\mathrm{ref}}_i$, with p_i denoting the partial pressure and 'ref' a reference state. We have chosen the reference state to be equal to the system's initial conditions with one exception; the reference state of chlorine is set to be its saturation concentration at 1 atm. i_0 is the exchange current density, T the absolute temperature and R the universal gas constant $E^{\mathrm{ref}}_{\mathrm{eq},j}$ is the potential difference between the solid and liquid phases at the reference state and at equilibrium conditions. Equation 25 and the condition of electroneutrality, Equation 24, provide the anode boundary conditions.

The following model equations are applied at the outer boundary surface, $\partial\Omega_r$:

$$\nabla c_i \cdot \mathbf{n} = 0 \quad (28)$$

$$\frac{1}{F}(\mathbf{i} \cdot \mathbf{n}) + \sum_i |z_i| u_i c_i (\nabla \boldsymbol{\Phi} \cdot \mathbf{n}) = 0 \quad (29)$$

where $\mathbf{i}$ is the total current density.

The initial concentrations are given by:

$$c_i(r, 0) = c^0_i \quad (30)$$

The initial potential at the anode surface, $\boldsymbol{\Phi}^0_{\mathrm{a}}$, is solved by Equation 26 with $i_1 = \mathbf{i}^0 \cdot \mathbf{n}$. The chlorine evolution reaction has no influence on $\boldsymbol{\Phi}^0_{\mathrm{a}}$ since no chlorine is present at the start of electrolysis. The initial potential profile, throughout the solution domain, is obtained by integrating Equation 29 using the boundary condition $\boldsymbol{\Phi}(r_{\mathrm{a}}, 0) = \boldsymbol{\Phi}^0_{\mathrm{a}}$.

5. Input data

All input parameters are valid at 37 °C. Initial concentrations of the nine species treated in this model are shown in Table 2. The physicochemical properties applied in the model are listed in Table 3. Standard electrode potentials are given as being relative to SHE. The geometrical dimensions of the anode and the electrolyte domain, used in all of the simulations, are $r_{\mathrm{a}} = 0.5$ mm and $r_r = 6$ cm. The value, r_r, was found to be large enough so as not to affect the solution of the problem.

5.1. *Initial concentrations*

The total ionic concentration of the aqueous solution is set to 0.16 M, and pH is set to 7.4. The bicarbonate

Table 2. Initial concentrations used in the model

Species	c^0_i/M
Na^+	0.16
H^+	$1 \times 10^{-7.4}$
Cl^-	0.133
OH^-	$1 \times 10^{-6.2}$
HCO_3^-	0.027
Cl_2(aq)	0
HClO	0
Org	0.28
Org–red	0.28

Table 3. Physicochemical input values to the model

Parameter	Value	Reference
$D_{Na^+}/cm^2\ s^{-1}$	1.78×10^{-5}	25
$D_{H^+}/cm^2\ s^{-1}$	12.5×10^{-5}	25
$D_{Cl^-}/cm^2\ s^{-1}$	2.72×10^{-5}	25
$D_{OH^-}/cm^2\ s^{-1}$	7.05×10^{-5}	25
$D_{HCO_3^-}/cm^2\ s^{-1}$	1.49×10^{-5}	25
$D_{Cl_2(aq)}/cm^2\ s^{-1}$	1.98×10^{-5}	26
$D_{HClO}/cm^2\ s^{-1}$	2.06×10^{-5}	27
$k_{4,f}/s^{-1}$	37	15
K_4/M^2	6.3×10^{-4}	15
$k_{6,7,8,9,f}/M^{-1}\ s^{-1}$	1×10^3	
$k_{11,f}/M^{-1}\ s^{-1}$	3.1×10^5	28
$k_{12,f}/M^{-1}\ s^{-1}$	1.5×10^{11}	29
K_w/M^2	$1 \times 10^{-13.6}$	30
c_{H_2O}/M	55.5	29
$c^S_{Cl_2(aq)}/M$	0.040	31
$i_{0,1}/A\ cm^{-2}$	1.0×10^{-10}	32
$i_{0,2}/A\ cm^{-2}$	1.0×10^{-3}	33
$E^{ref}_{eq,1}/V$	0.77	25
$E^{ref}_{eq,2}/V$	1.41	25

concentration in the model is set to 27 mM. These choices of concentration are justified by the fact that they are close to the actual concentrations found in plasma and interstitial fluid [21]. The initial hydroxyl ion concentration is calculated using the relation $c^0_{OH^-} = K_w/c^0_{H^+}$. To fulfil the electroneutrality condition, the exact initial sodium ion concentration is calculated by $c^0_{Na^+} = 0.16 - (c^0_{OH^-} - c^0_{H^+})$.

The capacity of tissue to chemically bond chlorine is estimated from a study made by Samuelsson and Jönsson, where the content of organically bound chlorine, in anodic lesions, was measured [22]. In their study, direct current was applied to normal lung tissue using two bullet-shaped platinum electrodes. After treatment, the content of organically bond chlorine in the grey–white centre of the anodic lesion was determined. The treated tissue contained, in the dried state, about 6% (w/w) covalently bond chlorine, while normal lung tissue contained approximately 1% (w/w). This elevation in chlorine content reflected the capacity of tissue to chemically bond chlorine and is recalculated into a molar concentration, c^0_{Org} (mole Org per dm^{-3} tissue), through the following equation:

$$c^0_{Org} = \frac{(x_{Cl,lesion} - x_{Cl,normal})x_{solid}\ \rho}{M_{Cl}} \tag{31}$$

where $x_{Cl,lesion}$ (w/w) is the dried chlorine content in the anodic lesions, $x_{Cl,normal}$ (w/w) the dried chlorine content in normal tissue and x_{solid} (w/w) the solid content in lung tissue. ρ denotes the density of tissue and M_{Cl} is the molar weight of elementary chlorine. The solid content in lung tissue is estimated to be 20% [21]. The density of tissue is approximated with the density of water, which is 0.99 g cm^{-3} at 37 °C [23].

The capacity of tissue to react with Cl_2(aq) and HClO through oxidation, or in other words the concentration of oxidizable organic substances $c^0_{Org-red}$, is not known. However, by making an analogy to a traditional application field of chlorine chemistry, namely pulp bleaching, it should be possible to make a fair estimation of tissue's reaction ability. This analogy is supported by the fact that in pulp bleaching, the specific chlorine consumption (g Cl_2 per g pulp) due to addition and substitution reactions is of the same order of magnitude as that obtained in EChT [22, 24]. Moreover, the bleaching process is run under similar time, temperature and pH conditions as EChT [24]. In pulp bleaching, the ratio of chlorination to oxidation is about 1:1 [18, 24], and this ratio has been used to estimate $c^0_{Org-red}$.

5.2. *Physicochemical properties*

Values for the diffusion coefficients at 37 °C were recalculated from values in water, at 25 °C, by using the following relationship [25]:

$$\frac{D_{25}\mu_{25}}{T_{25}} = \frac{D_{37}\mu_{37}}{T_{37}} \tag{32}$$

The viscosities are estimated to be $\mu_{25} = 0.890$ mN s m^{-2} and $\mu_{37} = 0.692$ mN s m^{-2} [23]. Org and Org–red are assumed to be immobile and therefore their diffusion coefficients are set to be close to zero. The ionic mobilities are related to the diffusion coefficients through the Nernst–Einstein equation [25].

The solubility of chlorine in tissue is estimated by Henry's law constant in pure water, and the constant a, in Equation 23, is set to 0.001. The forward rate constants of the reaction of chlorine with water and the water protolysis reaction are taken from literature, while the backward rate constants are obtained from $k_{4,b} = k_{4,f}/K_4$ and $k_{12,b} = K_w k_{12,f}/c_{H_2O}$, where K_4 is the equilibrium constant of Reaction 4. The forward rate constant of the buffer reaction is found in the literature and the product $k_{11,b}c_{CO_2(aq)}$ is calculated from the equilibrium expression of buffer Reaction 11 at initial conditions. Reactions 6–9 are generalizations of a myriad reactions, each with a specific rate constant from minimal size up to the order of $1 \times 10^9\ M^{-1}\ s^{-1}$ [19]. For simplicity, we assume in this work that the rate constants of Reactions 6–9, here denoted as $k_{6,7,8,9,f}$, are the same and equal to $1 \times 10^3\ M^{-1}\ s^{-1}$. The exchange current densities are estimated from experiments run in aqueous chloride solutions, while the equilibrium potentials are found through Nernst's equation.

6. Numerical implementation

The operator ∇ is written in spherical coordinates and, by assuming rotational symmetry, the model is reduced to a one-dimensional problem with the space coordinate r. The space derivatives are approximated by using the finite difference method. To avoid numerical problems, a new dimensionless space coordinate, x, is introduced.

$$x = \frac{r_r}{r}; \quad 1 \le x \le \frac{r_r}{r_a} \tag{33}$$

The transformation leads to shorter steps lengths close to the anode and longer step lengths further out in the electrolyte domain. By this procedure, the finite difference approximation is able to describe the large gradients at the anode surface. The mesh is uniform in the space coordinate x, and chosen so that no grid points appear on the boundaries. Two imaginary grid points are introduced at one half step lengths, $\Delta x/2$, outside the boundaries.

The time derivative is approximated by the trapezoidal rule. The obtained nonlinear equation system is solved by Newton's method [34], using sparse matrix routines included in Matlab®. The total number of grid points and the maximum time step were decided through ensuring convergence of the numerical solution, that is, when the refinement of the mesh and decrease of the time step did not affect the solution significantly.

7. Results and discussion

7.1. *General description of the simulated concentration profiles*

A simulation has been run in order to visualize the general behaviour of the simulated concentration profiles (Figures 2–4). The anode current density was, in this simulation, linearly raised from zero to 100 mA cm^{-2} in 2 min, and was subsequently kept constant during 30 min.

Figure 2 shows the simulated concentration profiles of sodium, hydrogen, chloride and bicarbonate ions at the end of this electrolysis. Hydrogen ions, produced in the oxygen evolution reaction and in the reactions of chlorine with tissue, form an acidic zone around the anode. The spreading of hydrogen ions is counteracted by these ions' reaction with bicarbonate. Chloride is consumed in the chlorine evolution reaction, which results in depletion of chloride ions adjacent the anode. The sodium ions are transported away from the anode by means of migration. The concentration profiles of all ions are closely related through the electroneutrality condition.

Simulated concentration profiles of chlorine, hypochlorous acid and reactive organic sites, after different times of this electrolysis, are shown in Figure 3. Chlorine, produced in the chlorine evolution reaction, diffuses away from the anode. and its profile reaches a maximum plateau due to saturation. Some of the chlorine hydrolyses into hypochlorous acid, which also diffuses away from the anode. The fact that the concentration profiles of chlorine, hypochlorous acid and the organic constituents all meet in a very narrow reaction zone implies that Reactions 6–9 are diffusion-controlled.

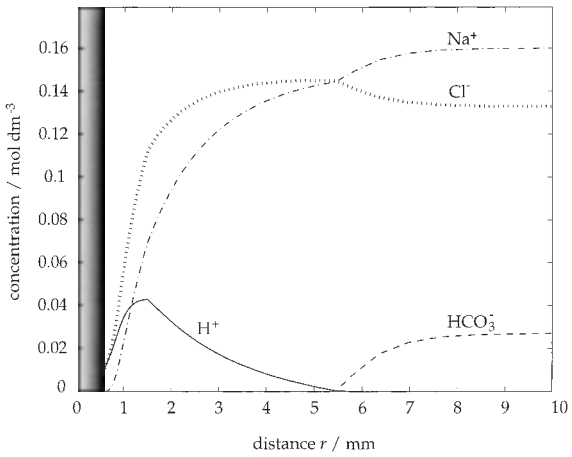

Fig. 2. Simulated concentration profiles of sodium, hydrogen, chloride and bicarbonate ions. Anode current density, in this simulation, linearly raised from zero to 100 mA cm^{-2} in 2 min, and subsequently kept constant during 30 min.

Figure 4 shows the simulated pH profile around the anode after different times of electrolysis. Throughout the electrolysis, the profiles shifts sharply from acidic to neutral while the local minimum, in pH, basically remains constant. As can be seen by comparing Figures 3 and 4, the acidic zone surrounding the anode is much larger than the chlorinated zone. Consequently at these specific treatment conditions, the simulation clearly indicates that it is the spreading of hydrogen ions – and not chlorine – that determines the extent and size of the destruction zone around the anode.

7.2. *Influence of current density on chlorination and acidification*

Calculations have been done using a broad range of anode current densities ranging from 5 to 150 mA cm^{-2} (Figures 5–8). In all simulations, the current density was linearly raised from zero to operating current density in

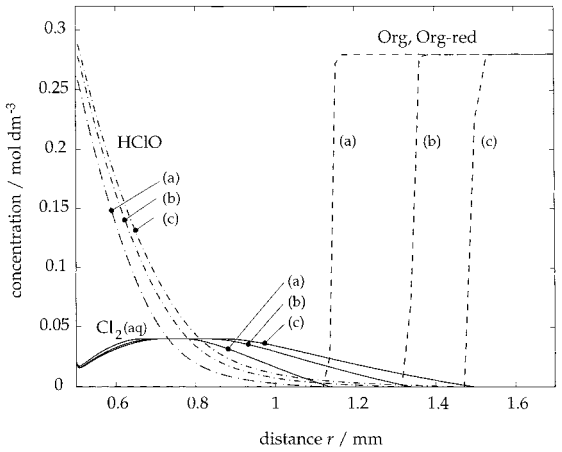

Fig. 3. Simulated concentration profiles of chlorine, hypochlorous acid and reactive organic sites, after different times of electrolysis: (a) 2 + 10 min, (b) 2 + 20 min and (c) 2 + 30 min. Anode current density, in this simulation, linearly raised from zero to 100 mA cm^{-2} in 2 min, and subsequently kept constant during 30 min.

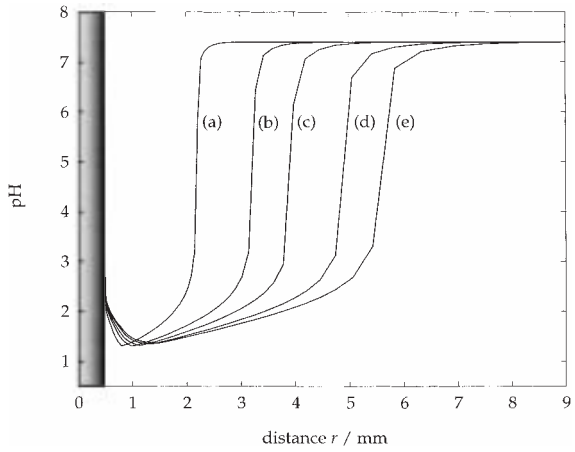

Fig. 4. Simulated pH profiles around the anode after different times of electrolysis: (a) 2 + 1 min, (b) 2 + 5 min, (c) 2 + 10 min, (d) 2 + 20 min and (e) 2 + 30 min. Anode current density, in this simulation, linearly raised from zero to 100 mA cm^{-2} in 2 min, and subsequently kept constant during 30 min.

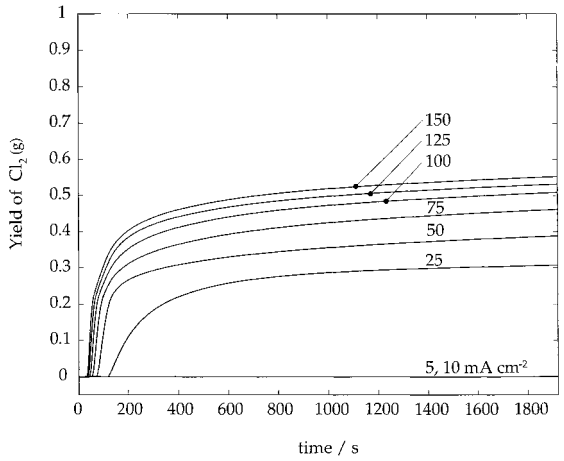

Fig. 6. Simulated release of chlorine into the gas phase, as a function of time at different anode current densities: 5, 10, 25, 50, 75, 100, 125 and 150 mA cm^{-2}. Chlorine loss is defined as the normalized part of total amount of chlorine produced at anode that is lost to gas phase. Anode current density, in this simulation, linearly raised from zero to operating current in 2 min, and subsequently kept constant during 30 min.

2 min, and was subsequently kept constant during 30 min.

Figure 5 shows the extension of the chlorinated and acidic zones, in tissue surrounding the anode, as functions of current density. The extension of the acidic zone is plotted for pH values of 2, 3 and 7. The radii corresponding to these pH values are obtained from individual pH profiles at different current densities. The simulations show that the size of the acidic zone increases significantly with increasing current density. On the other hand, the chlorinated zone increases only slightly with increasing current density. In fact, at current densities higher than 75 mA cm^{-2}, the radius of the chlorinated zone is almost constant. The explanation for this behaviour is that tissue already becomes saturated with chlorine at low current densities, so that subsequent produced chlorine is lost to the gas phase as current density increases. Figure 6 shows the normalized part of

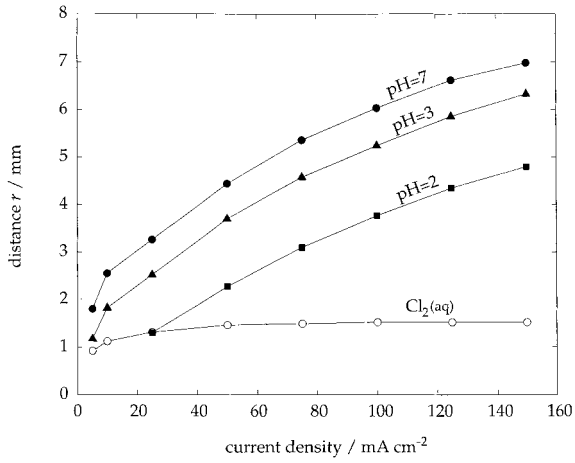

Fig. 5. Simulated extensions of chlorinated and acidic zones around the anode, as functions of current density. Extension of acidic zone is plotted for pH values of 2, 3 and 7. Anode current density, in this simulation, linearly raised from zero to operating current in 2 min, and subsequently kept constant during 30 min.

the total amount of chlorine produced at the anode, that is released to the gas phase, as a function of time at different total current densities. At the two lowest current densities of 5 and 10 mA cm^{-2}, the rate of production of chlorine is low enough to avoid saturation.

Generally, it can be stated that the outer boundary of the acidic zone is always ahead of the boundary of the chlorinated zone. This does not necessarily mean that it is always the hydrogen ion that plays the role as principal destructive agent. It most probably takes a pH of between 2 and 3 to cause irreversible tissue destruction [10, 35, 36]. Moreover, the pH needed to cause irreversibly cell damage may also be dependent on the time of exposure [8, 37]. Figure 5 shows that the hydrogen ion is the principal destructive agent at current densities higher than 25 mA cm^{-2}, assuming that $pH < 2$ causes lesions. At lower current densities, the spreading of chlorine and hypochlorous acid determines the size of the destruction zone. If, instead, $pH < 3$ is used as the destruction condition, then the simulations indicate that it is the acidification that causes tissue destruction, irrespective of the applied current density.

Secondary reactions, arising from the chlorine production at the anode, play important roles as generators of hydrogen ions. Figure 7 shows the normalized contribution to the total production of hydrogen ions from the reactions of chlorine with tissue (i.e., Reactions 4, 6, 8 and 9) as a function of time at different current densities. Chlorine is responsible for as much as 97% of the acidification surrounding the anode, at the two lowest current densities of 5 and 10 mA cm^{-2}. The impact that chlorine has on acidification around the anode is considerably decreased with increasing current density. The reason for this is that the current yield of chlorine varies with applied current density. The normalised part of the total current density, contributed by the chlorine evolution reaction, is plotted in Figure 8 as a function of time at

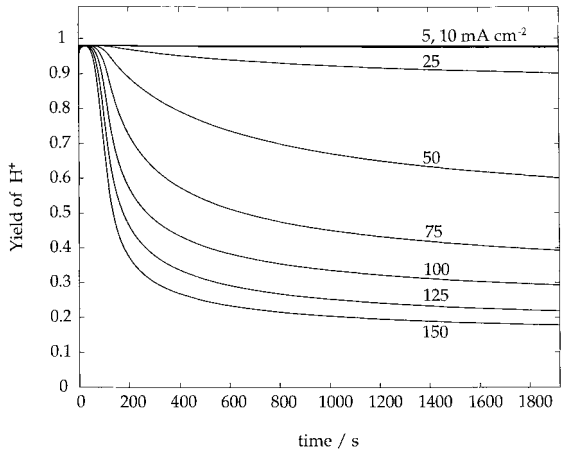

Fig. 7. Simulated normalized contributions from the reactions of chlorine with tissue (i.e., Reactions 4, 6, 8 and 9) to total production of hydrogen ions, as a function of time at different anode current densities: 5, 10, 25, 50, 75, 100, 125 and 150 mA cm^{-2}. Anode current density, in this simulation, linearly raised from zero to operating current in 2 min, and subsequently kept constant during 30 min.

different total current densities. At low current densities, in the absence of mass transport limitations, the chlorine evolution reaction is kinetically favoured by its high exchange current density. When the current density is increased, the chlorine evolution reaction becomes diffusion-limited and its current yield decreases significantly.

There is a large difference between our simulated current yields and the current yields reported in an experimental study made by Samuelsson and Jönsson [22]. They investigated the chlorine current yield at a platinum foil anode, immersed in physiological saline solution. The experiments were run in a gas-tight cell and the released chlorine was determined by iodometric titration. A broad range of current densities, ranging from 5 to 130 mA cm^{-2}, was investigated. The chlorine yield was found to vary in between 37% and 50%, with

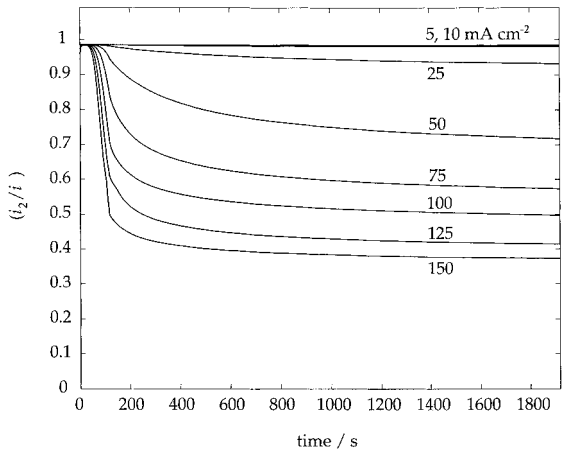

Fig. 8. Simulated normalized contributions from the chlorine evolution reaction, to the total anode current density, as a function of time at different total current densities: 5, 10, 25, 50, 75, 100, 125 and 150 mA cm^{-2}. Anode current density, in this simulation, linearly raised from zero to operating current in 2 min, and subsequently kept constant during 30 min.

a maximum yield occurring at 40 mA cm^{-2}. The poor agreement between the simulated and the experimentally measured current yields is caused by two serious shortcomings in their experimental design. First, no consideration was taken to the fact that a large part of the produced chlorine shows up as hypochlorous acid and, hence, the measured current yields does not reflect the actual current yield obtained in the experiments. Secondly, convection was allowed to enhance mass transport around the anode. In real EChT treatments, the principal transport mechanisms are diffusion and migration as convection is strongly obstructed by the dense structure of tissue.

It is important to note that, except for the two lowest current densities, the yield of hydrogen ions originating from the reactions of chlorine with tissue is significantly less than the corresponding current yield of chlorine, see Figures 7 and 8. This can partly be explained by comparing the number of hydrogen ions produced, per transferred electron in the chlorine and oxygen evolution reactions, respectively. One hydrogen ion is produced per transferred electron in the oxygen evolution reaction. The chlorinating reactions (6) give rise to a net production of half a hydrogen ion per transferred electron, from the chlorine evolution reaction, while the oxidation reactions (8) and (9) correspond to a net production of one hydrogen ion. In addition, the production of hypochlorous acid (4) alone, without subsequent reactions with organic constituents, generates a half hydrogen ion per transferred electron in the chlorine evolution reaction. This comparison, together with the fact that a large part of the chlorine is lost to the gas phase, clearly shows that the acidifying power of the chlorine evolution reaction is, although not negligible, considerably less than that of oxygen evolution.

7.3. *Sensitivity analysis*

The estimations contained in the capacity of the tissue to react with chlorine and hypochlorous acid, through oxidation, $c^0_{\text{Org–red}}$, and the rate constant of Reactions 6–9, $k_{6,7,8,9,f}$, are both impaired with large uncertainties. Accordingly, calculations have been run using a wide spectrum of $c^0_{\text{Org–red}}$ and $k_{6,7,8,9,f}$, so that their influence on the simulation results can be thoroughly investigated (Figures 9–11). In all of the simulations, current density was linearly raised from zero to an operating current density in 2 min, and was subsequently kept constant during 30 min.

Figure 9 shows the simulated concentration profiles of chlorine and hydrogen ions, when using different values of $c^0_{\text{Org–red}}$. The anode current density in these simulations was set of 100 mA cm^{-2}. The oxidation reactions provide an important source of hydrogen ions, which results in a maximum hydrogen ion concentration, localized at the reaction front of chlorine, that increases with increasing $c^0_{\text{Org–red}}$. However, the extension of the acidic zone is only slightly affected by $c^0_{\text{Org–red}}$. The consumption of chlorine by Org–red increases with

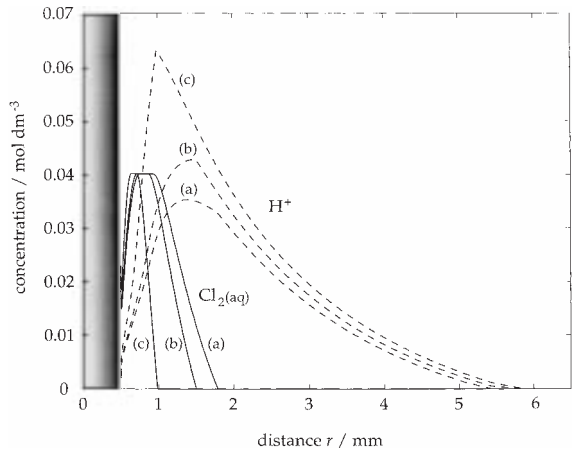

Fig. 9. Simulated concentration profiles of chlorine and hydrogen ions at different values on $c^0_{\text{Org–red}}$: (a) 0, (b) 0.28 and (c) 2.8 M. Anode current density, in this simulation, linearly raised from zero to 100 mA cm^{-2} in 2 min, and subsequently kept constant during 30 min.

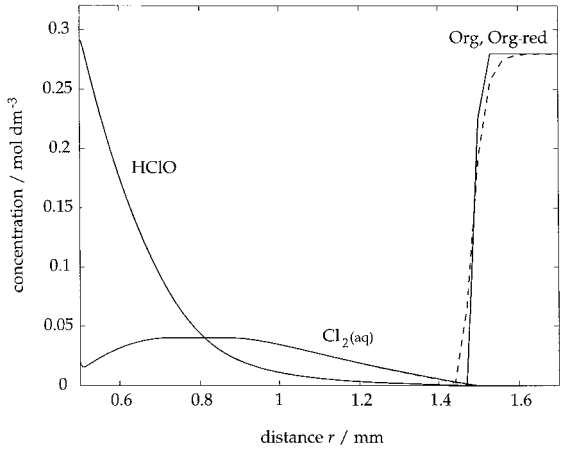

Fig. 11. Simulated concentration profiles of chlorine, hypochlorous acid and reactive organic sites, at different values on $k_{6,7,8,9,f}$: 10 (- - -) 1×10^3 (——) and 1×10^5 (- · -) M^{-1} s^{-1}. Anode current density, in this simulation, linearly raised from zero to operating current in 2 min, and subsequently kept constant during 30 min.

increasing $c^0_{\text{Org–red}}$ and, consequently, the spreading of chlorine is impeded.

The influence of $c^0_{\text{Org–red}}$ on the simulated pH profile becomes more prominent at lower current densities, see Figure 10. At 10 mA cm^{-2}, oxidation reactions are the main source of acidification surrounding the anode and both the acidity and the extension of the acidified zone are affected by $c^0_{\text{Org–red}}$.

The concentration profiles of chlorine, hypochlorous acid and reactive organic sites, using different values on the rate constant of Reactions 6–9, $k_{6,7,8,9,f}$, are shown in Figure 11. The anode current density in this simulation was set to 100 mA cm^{-2}. The simulations clearly show that the spreading of chlorine and hypochlorous acid is controlled by diffusion. Although $k_{6,7,8,9,f}$ is varied within four orders of magnitude, the concentration profiles of chlorine and hypochlorous acid remain unchanged.

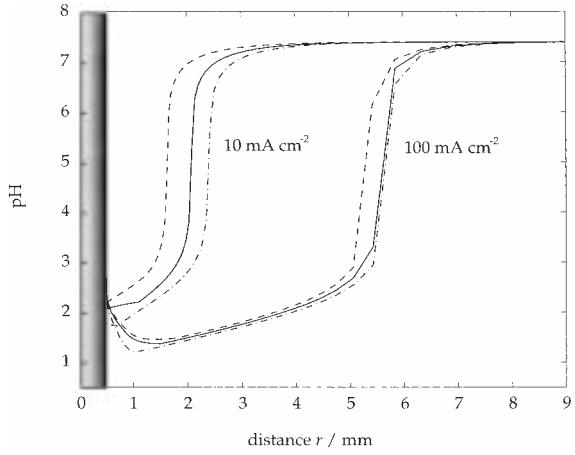

Fig. 10. Simulated pH profiles at different current densities (10 and 100 mA cm^{-2}) and different values on $c^0_{\text{Org–red}}$: 0 (- - -) 0.28 (——) and 2.8 (- · -) M. Anode current density, in this simulation, linearly raised from zero to operating current in 2 min, and subsequently kept constant during 30 min.

7.4. *Comparison between simulations and experimental results*

The validity of the model is evaluated by comparing simulated results with results obtained after EChT treatment of normal mammary tissue in rats [6]. In the experiments, constant direct current was applied to the tissue by means of two spherical Pt:Ir (9:1) electrodes, with a radius of 0.5 mm. Three different currents were used in the experiment, corresponding to anode current densities of 34, 85 and 171 mA cm^{-2}. In the experiments, current was linearly raised from zero to operating current in 2 min, and was similarly decreased to zero at the end of the treatment. The treatment times were adjusted so that, in each of the experiments, a total charge of 5 *C* was passed between the electrodes. The diameter of the spherical dark brown lesion, produced around the anode, was measured directly after treatment. A diffuse grey–white zone, caused by the reactions of chlorine and hypochlorous acid with tissue, was obtained within the dark brown lesion. Subsequently, pH measurements were performed with a microcombination pH electrode. Measurements were made in the centre of the lesion, and at every second mm from this point, until well out into the region of healthy tissue. The last pH measurement, in the tissue surrounding the anode, was run about 10–15 min after current shutdown.

Simulations were run using current densities and treatment times identical to those used in the experiments. Simulations, in which i_1, i_2 and $\nabla\mathbf{\Phi}$ were set to zero after current shutdown, were also run. In this way, the diffusion-reaction processes occurring between current shutdown and pH measurement could also be modelled.

The simulated pH profiles, obtained immediately after current shutdown and after 10 and 15 min of mass transport, are presented in Figure 12. Also shown in

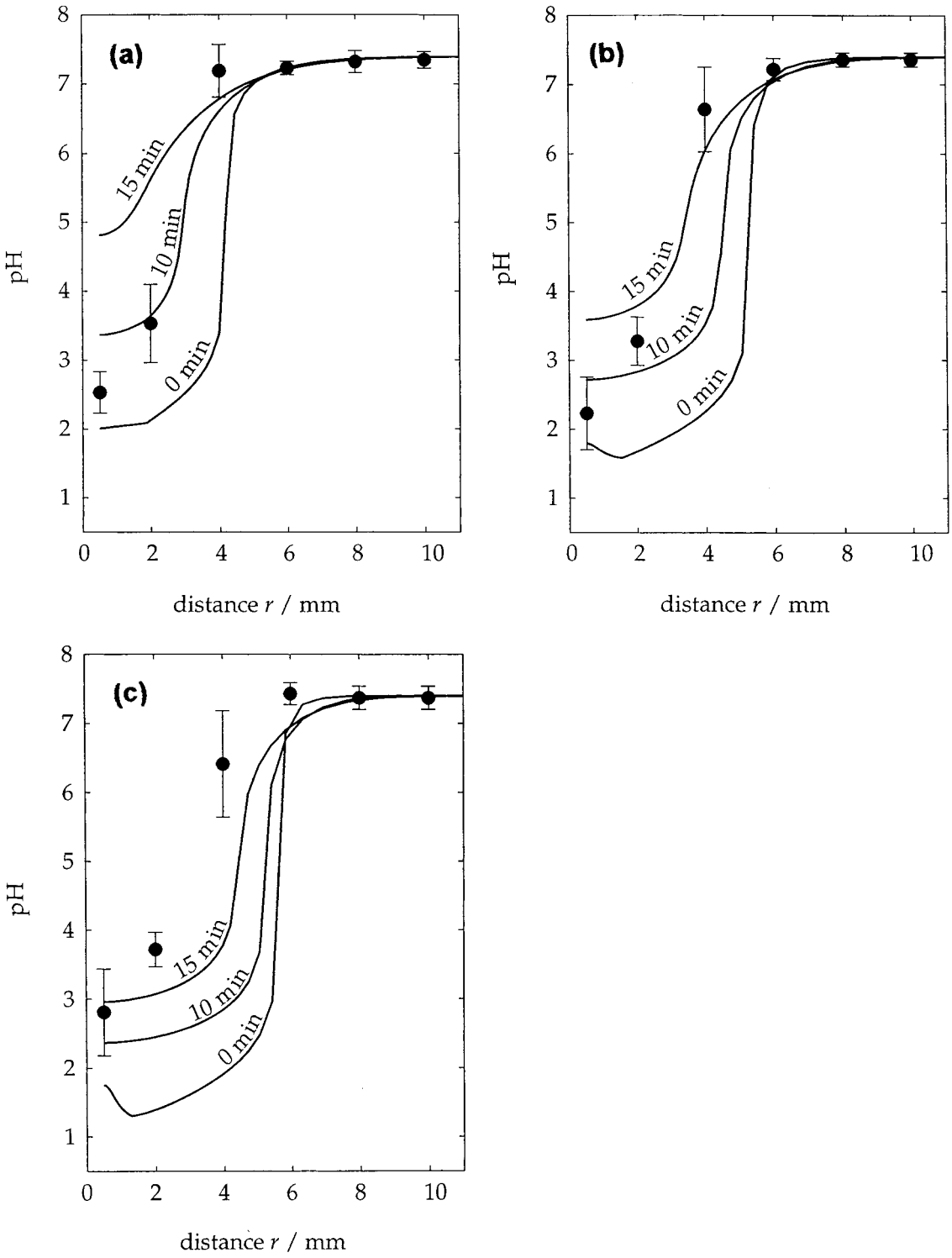

Fig. 12. Comparison between simulated and experimental pH profiles [6] at different treatment conditions: (a) 1, (b) 2.5 and (c) 5 mA. Treatment times adjusted so that, in each of the experiments, a total charge of 5 C was passed between the electrodes. Experimental values (●) given as the mean ± 1 standard deviation. Simulated pH profiles (—) presented as a function of time: 0, 10 and 15 min following current shutdown.

Figure 12 are the experimentally measured pH profiles, which agree well with the simulated profiles. The slight difference in shape between simulated and experimental profiles could possibly be explained by an underestimation of tissue's buffer capacity and/or an overestimation of the buffer reaction rate. The model's ability to predict the pH profile in tissue surrounding the anode, within a wide range of currents, strongly supports its general validity.

The correlation between the experimentally measured lesions and the simulated size of the chlorinated zone is shown in Table 4. Also presented in the table is the simulated pH obtained at a radius corresponding to the border of the experimental lesions. These pH values

Table 4. Experimental lesion radii (mean ± 1 standard deviation) [6], simulated radii of the chlorinated zone and simulated pH values at the radius corresponding to the border of the experimental mean lesion radii, at different treatment conditions

Treatment conditions	Experimental lesion radius /mm	Simulated radius of the chlorinated zone/mm	Simulated pH at experimental lesion border
1 mA, 5 C	2.7 ± 0.5	1.9	2.3
2.5 mA, 5 C	3.5 ± 0.4	1.5	2.0
5 mA, 5 C	3.4 ± 0.3	1.3	1.7

were found just before the current was decreased to zero in the final 2 min run. As can be seen in the table, the experimental lesion radii are larger than the simulated radii of the chlorinated zones, in all treatment groups. Furthermore, the simulated pH at the border of the experimental lesions correlates well to a value around 2. These two findings are both in line with the results presented earlier in Section 7.2; namely that at this present range of current densities, the size of the destruction zone is determined by the spreading of hydrogen ions.

It should be noted that boundaries in the simulated profiles, of organically bonded chlorine, are sharper than the corresponding grey–white zone border, obtained in the experiments. This can be explained by the fact that the model only accounts for one rate constant, in the reactions of chlorine and hypochlorous acid with organic matter. In reality, a number of reactions, with largely varying rate constants, are present.

8. Conclusion

The mathematical model presented in this study increases the understanding of the role of chlorine in the underlying destruction mechanisms behind EChT treatments. A considerable amount of the chlorine, produced at the anode, reacts with water to form hypochlorous acid. Chlorine and hypochlorous acid are potent chlorinating and oxidising agents, with strongly toxic properties. Their impact in the overall destruction mechanism is, however, found to be very limited since the acidic zone always reaches further out from the anode than the chlorinated zone. Except for the case of very low anode current densities, the simulations clearly show that it is the spreading of the hydrogen ion that determines the extent of tissue destruction around the anode.

Although chlorine and hypochlorous acid themselves are found to have limited roles in the destruction mechanism of EChT, their secondary reactions with tissue are shown to be important sources for production of hydrogen ions. The contribution of these reactions to the acidification of tissue surrounding the anode is strongly dependent on the applied current density and increases with decreasing current density.

Acknowledgements

This work was financially supported by The Swedish Cancer Society. The working group for 'Analysis of mechanisms of electrochemical treatment of cancer' including The Royal Institute of Technology, Radiumhemmet, The Swedish University of Agricultural Sciences and Huddinge University Hospital, is acknowledged for their co-operation and valuable discussions. Philip Byrne is acknowledged for valuable opinions on the manuscript.

References

1. B.E.W. Nordenström, 'Biologically Closed Electrical Circuits: Clinical, Experimental and Theoretical Evidence for an Additional Circulatory System' (Nordic Medical Publications, Stockholm, 1983).
2. D. Miklavčič, G. Serša, M. Kryžanowski, S. Novakovič, F. Bobanović, R. Golouh and L. Vodovnik, *Bioelectrochem. Bioenerg.* **30** (1993) 209.
3. K-H. Li, Y-L. Xin, Y-N. Gu, B-I. Xu, D-J. Fan and B-F. Ni, *Bioelectromagnetics* **18** (1997) 2.
4. L. Samuelsson, T. Olin and N.O. Berg, *Acta Radiol.* **21** (1980) 447.
5. T. Jarm, M. Čemažar, G. Serša and D. Miklavčič, *Electro. Magnetobiol.* **17** (1998) 273.
6. H. von Euler, E. Nilsson, A-S. Lagerstedt and J.M. Olsson, *Electro. Magnetobiol.* **18** (1999) 93.
7. Y-L. Xin, *Eur. J. Surg. Suppl.* **574** (1994) 31.
8. Y-L. Xin, F-Z. Xue, B-S. Ge, F-R. Zhao, B. Shi and W. Zhang, *Bioelectromagnetics* **18** (1997) 8.
9. Y-L. Xin, The clinical advance in application of EChT within the past ten years, Preprints from the 2nd international symposium on electrochemical treatment of cancer, 27–30 Sept., Beijing, China (1998), p. 81.
10. E. Nilsson, J. Berendson and E. Fontes, *Bioelectrochem. Bioenerg.* **47** (1998) 11.
11. E. Nilsson, J. Berendson and E. Fontes, *J. Electroanal. Chem.* **460** (1999) 88.
12. L. Samuelsson, I-L. Lamm, C.E. Mercke, E. Ståhl and L. Jönsson, *Acta Radiol.* **26** (1985) 521.
13. J. Berendson and D. Simonsson, *Eur. J. Surg. Suppl.* **574** (1994) 111.
14. J. Berendson and J.M. Olsson, *Electro. Magnetobiol.* **17** (1998) 1.
15. S.S. Ashour, E.B. Rinker and O.C. Sandall, *AIChE J.* **42** (1996) 671.
16. G.C. White, 'Handbook of Chlorination' (Van Nostrand Reinhold, New York, 1986).
17. T.W.G. Solomons, 'Organic Chemistry', 4th edn (J. Wiley & Sons, New York, 1988).
18. K.R. Solomon, *Pure & Appl. Chem.* **68** (1996) 1721.
19. L.W. Hall Jr., G.R. Helz, D.T. Burton and J. Huckabee, 'Power plant Chlorination' (Ann Arbor Science, Ann Arbor, 1981).
20. R.L. Jolley, G. Jones, W.W. Pitt and J.E. Thompson, Chlorination of organics in cooling waters and process effluents, *in* R.L. Jolley (ed.), 'Water Chlorination: Environmental Impact and Health Effects', Vol. 1 (Ann Arbor Science, Ann Arbor, 1978).
21. J.B. West, 'Physiological Basis of Medical Practice', 11th edn (William & Wilkins, Baltimore, 1985).
22. L. Samuelsson and L. Jönsson, *Acta Radiol.* **21** (1980) 711.
23. R.C. West, 'Handbook of Chemistry and Physics', 54th edn (CRC Press, Ohio, 1974).
24. S. Rydholm, 'Pulping Processes' (J. Wiley & Sons, New York, 1965).
25. J.S. Newman, 'Electrochemical Systems', 2nd edn (Prentice-Hall, Englewood Cliffs, NJ, 1991).

26. C.W. Spalding, *AIChE J*. **8** (1962) 685.
27. H. Hikita, S. Asai, Y. Himukashi and T. Takatsuka, *Chem. Eng. J*. **5** (1973) 77.
28. 'Gmelin's Handbuch der Anorganischen Chemie', Kohlenstoff, Teil C3, System nr. 14 (Verlag Chemie, Weinheim, 1973).
29. W.J. Moore, 'Basic Physical Chemistry' (Prentice-Hall International Editions, London, 1983).
30. O. Siggard-Andersen, 'The Acid–Base Status of the Blood', 4th edn (Munksgaard, Copenhagen, 1974).
31. G. Ruiz-Ibanez, A. Bidarian, R.A. Davis and O.C. Sandall, *J. Chem. Eng. Data* **36** (1991) 459.
32. A. Damjanovic, V.I. Birss and D.S. Boudreaux, *J. Electrochem. Soc*. **138** (1991) 2549.
33. A.J. Bard, 'Encyclopedia of Electrochemistry of the Elements', Vol. 1 (Marcel Dekker, New York, 1973).
34. G. Dahlquist and Å. Björck, 'Numerical Methods' (Prentice-Hall, Englewood Cliffs, NJ, 1974).
35. H. Ito and S. Hashimoto, *J. Jpn. Soc. Cancer* **23** (1988) 696.
36. R. Lemberg and M. Legge, 'Hematin Compounds and Bile Pigments' (Interscience, New York, 1949).
37. Y. Yen, J-R. Li, B-S. Zhou, F. Rojas, J. Yu and C.K. Chou, *Bioelectromagnetics* **20** (1999) 34.